EUROPHYSICS LETTERS 15 April 2004

Europhys. Lett., **66** (2), pp. 232–238 (2004)
DOI: 10.1209/epl/i2003-10183-2

Spectroscopic measurements of phase-resolved electron energy distribution functions in RF-excited discharges

T. Gans[1](*), V. Schulz-von der Gathen[2] and H. F. Döbele[2]

[1] *Ruhr-Universität Bochum, Institut für Plasma- und Atomphysik 44780 Bochum, Germany*(**)
[2] *Universität Duisburg-Essen, Institut für Laser- und Plasmaphysik 45117 Essen, Germany*

(received 20 October 2003; accepted in final form 6 February 2004)

PACS. 52.70.-m – Plasma diagnostic techniques and instrumentation.
PACS. 52.70.Kz – Optical (ultraviolet, visible, infrared) measurements.
PACS. 52.80.Pi – High-frequency and RF discharges.

Abstract. – The reliable measurement of the electron energy distribution function (EEDF) of plasmas is one of the most important subjects of plasma diagnostics, because this piece of information is the key to understand basic discharge mechanisms. Specific problems arise in the case of RF-excited plasmas, since the properties of electrons are subject to changes on a nanosecond time scale and show pronounced spatial anisotropy. We report on a novel spectroscopic method for phase- and space-resolved measurements of the electron energy distribution function of energetic ($> 12\,\mathrm{eV}$) electrons in RF discharges. These electrons dominate excitation and ionization processes and are therefore of particular interest. The technique is based on time-dependent measurements during the RF cycle of excited-state populations of rare gases admixed in small fractions. These measurements yield —in combination with an analytical model— detailed information on the excitation processes. Phase-resolved optical emission spectroscopy allows us to overcome the difficulties connected with the very low densities (10^7–$10^9\,\mathrm{cm}^{-3}$) and the transient character of the electrons in the sheath region. The EEDF of electrons accelerated in the sheath region can be described by a shifted Maxwellian with a drift velocity component in direction of the electric field. The method yields the high-energy tail of the EEDF on an absolute scale. The applicability of the method is demonstrated at a capacitively coupled RF discharge in hydrogen.

The electron energy distribution function (EEDF) is of primary importance for the understanding of basic RF discharge mechanisms like electron heating, dissociation, excitation and ionization. High-energy electrons play the dominant role in these processes. Optical emission spectroscopy (OES) has been successfully applied to the measurements of EEDFs under steady-state conditions [1, 2]. Populations of states excited by electrons from different

(*) E-mail: Timo.Gans@web.de
(**) Present address.

energy ranges of the EEDF are usually compared. A suitable mixture of rare gases is added to the discharge to provide a broad basis of states of different excitation energy. In the case of RF-excited plasmas, time-resolved measurements have revealed substantial changes in the line intensities within the RF discharge cycle indicating changes in the high-energy tail of the EEDF [3]. EEDFs are commonly determined in plasmas of this density range with Langmuir probes [4, 5]; these cannot provide, however, the necessary time resolution on a time scale below $\sim$ 10 ns. Thomson scattering has become popular in the last few years also for RF discharges [6].

This method has inherent time resolution —it is, however, by far not sensitive enough to allow the extension to the very low number densities of the electrons populating the high-energy tail of the EEDF. We can, therefore, conclude that no reliable quantitative diagnostic method has been existing so far to measure the EEDF in the time-dependent high-energy tail.

In this work, the spectroscopic approach is extended to phase- and space-resolved measurements of transient, energetic, directed electrons in RF discharges. The required analytical model for the population dynamics within the RF cycle and an analytical approach for the EEDF are discussed below. This novel diagnostic became possible by the availability of improved data on electron impact excitation cross-sections, cascading contributions from higher electronic states and coefficients for radiation-less collisional de-excitation (quenching) measured recently in electron beam [7–10] and other PROES (phase-resolved optical emission spectroscopy) experiments [11]. After the description of the diagnostic technique, its applicability is demonstrated at a capacitively coupled RF (CCRF) discharge in hydrogen with pronounced excitation dynamics and broad application potential.

In contrast to the standard corona model commonly used to calculate intensity ratios in stationary low-density plasmas, a time-dependent model based on rate equations is needed in this case to cope with the transient character of electronic excitation. Electron impact ($E^{\mathrm{e}}(t)$) and heavy-particle collisional excitation ($E^{\mathrm{H}}(t)$) out of the ground state are described by the excitation function $E(t) = E^{\mathrm{e}}(t) + E^{\mathrm{H}}(t)$. Excitation out of metastable or resonant atomic states is negligible in molecular discharges at elevated pressure —such as the hydrogen CCRF discharge investigated— because of low population densities of these states due to effective quenching processes by molecules [12]. For an excited state i not populated by cascade processes, the excitation function $E_i(t)$ can be determined directly from the measured number of photons per unit volume and time $\dot{n}_{\mathrm{Ph},i}(t)$:

$$E_i(t) = \frac{1}{n_0 A_{ik}} \left(\frac{\mathrm{d}\dot{n}_{\mathrm{Ph},i}(t)}{\mathrm{d}t} + A_i \dot{n}_{\mathrm{Ph},i}(t) \right). \tag{1}$$

Here, $\dot{n}_{\mathrm{Ph},i}(t) = A_{ik} n_i(t)$ is given by the transition probability A_{ik} of the observed emission and the population of the investigated state $n_i(t)$; n_0 is the ground-state density. The effective decay rate $A_i = \sum_k A_{ik} g_{ik} + \sum_q k_q n_q$ takes account of spontaneous emission, radiation trapping and quenching, where g_{ik} is the so-called escape factor and k_q the quenching coefficient with the species q of the density n_q. For quantitative investigations of the population dynamics, cascade processes can be substantial [7–11]. The population density $n_i(t)$ of the investigated state i can be described by the following rate equation including cascades from state c:

$$\frac{\mathrm{d}n_i(t)}{\mathrm{d}t} = n_0 E_i(t) - A_i n_i(t) + A_{ci} n_c(t). \tag{2}$$

The population density $n_c(t)$ obeys a rate equation analogous to eq. (2), without cascade processes. The coupled differential equations for the investigated state i and the cascade state c can be solved in a general manner for the periodic boundary conditions of an RF discharge

$(n_{i,c}(t) = n_{i,c}(t+T))$:

$$\begin{aligned} n_i(t) \;=\; & n_0\left(\frac{\widetilde{E_i}(T,A_i)e^{-A_iT}}{1-e^{-A_iT}} + \widetilde{E_i}(t,A_i)\right)e^{-A_it} + \\ & + \frac{n_0 A_{ci}}{A_i - A_c}\left[\left(\frac{\widetilde{E_c}(T,A_c)e^{-A_cT}}{1-e^{-A_cT}} + \widetilde{E_c}(t,A_c)\right)e^{-A_ct} - \right. \\ & \left. - \left(\frac{\widetilde{E_c}(T,A_i)e^{-A_iT}}{1-e^{-A_iT}} + \widetilde{E_c}(t,A_i)\right)e^{-A_it}\right]. \end{aligned} \tag{3}$$

Here, the abbreviation $\widetilde{E_x}(t,A_y) = \int_0^t E_x(t')e^{A_yt'}\mathrm{d}t'$ has been used. Together with analytical approximations for time dependencies of excitation processes, eq. (3) allows us to determine amplitudes of excitation processes even for states fed by cascade processes. Furthermore, this access to excitation functions is less sensitive to noise in measurements than the direct one (eq. (1)), because derivatives of measured data are avoided.

The following atomic states turned out to be well suited to the determination of EEDFs: Kr $2p_5$, Kr $2p_2$, Ar $2p_1$, Ne $2p_6$, Ne $2p_1$, He 3^3S and He 3^1S. These states have excitation thresholds in the range from 11.7 eV to 22.9 eV and their electron impact excitation cross-sections as well as the contributions of cascades are accurately known [7–10]. The comparatively small cascade contribution to the population of these states justifies the neglect of second-order cascade processes. The effective lifetimes of the states $1/A_i$, taking account of quenching, are shorter than the RF period which allows one to observe excitation dynamics within the RF cycle. Comparison of measured excitation functions of these states yields information on the EEDF in an energy range even beyond the different excitation thresholds because of different shapes of the electron impact excitation cross-sections, in particular for the singlet and triplet states of He. The gained information does not provide a direct access to the EEDF, since the excitation function E_i^{e} is given by the integral over the energy-dependent electron impact excitation cross-section $\sigma_i(E)$ and the EEDF $f(E)$:

$$E_i^{\mathrm{e}} = n_{\mathrm{e}}\int_0^\infty \sigma_i(E)\sqrt{\frac{2E}{m_{\mathrm{e}}}}f(E)\mathrm{d}E. \tag{4}$$

Here, n_{e} and m_{e} are the electron density and mass, respectively. This problem can be overcome by devising a reasonable analytical approach with a set of free parameters describing the shape of the EEDF. This set is varied until the EEDF reproduces best the measured excitation functions of all states under consideration.

The common approach to an EEDF is a Maxwellian or a Druyvesteynian distribution function with the electron temperature as the only parameter. In ref. [1] a more general approach including both cases is proposed by introducing a second free parameter. In the general case an approach adapted to the symmetry of the discharge under consideration is required. An example that requires the modification of the isotropic distribution functions mentioned is the acceleration of electrons by electric fields in axial direction. This modification will apply to discharges with sheaths —see below.

The experimental verification of the diagnostic technique presented was conducted at a hydrogen CCRF discharge. The setup is described in detail elsewhere [13]. The flat cooled stainless-steel electrodes, 100 mm in diameter, are 25 mm apart. The discharge is excited asymmetrically with one electrode grounded. The discharge axis is imaged onto the entrance slit of a 2 m spectrograph. A fast gateable ICCD-camera (LaVision Picostar, gate: 3 ns, repetition rate: 13.56 MHz) samples spectral intervals of about 4.5 nm with a spectral resolution

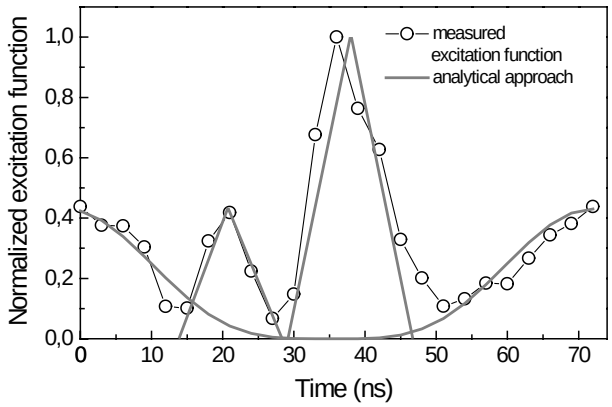

Fig. 1 – Excitation function of the neon $2p_1$ state close to the sheath boundary (approximately 4 mm in front of the powered electrode) including analytical approximations for excitation during the field-reversal phase, the sheath expansion phase and by secondary electrons.

of 0.03 nm and a spatial resolution of about 0.5 mm. The wavelength-dependent sensitivity of the entire optical system is calibrated with a tungsten ribbon lamp allowing for absolute measurements of the EEDF. The measurements are performed at an RF power of 100 W and a total gas pressure of 148 Pa. A small amount (5%) of a rare-gas mixture (10% Kr, 20% Ar, 30% Ne, 40% He) is added to the hydrogen discharge. Unequal proportions are used, since the influence of rare-gas admixtures on the investigated discharge was found to increase with decreasing ionization energy of the rare gas. For admixtures of tracer gases $< 5\%$, no influence was observable. Transition rates of the investigated rare-gas states and coefficients for quenching with molecular hydrogen are taken from ref. [11] and ref. [14], respectively.

Various electron impact and heavy-particle collisional excitation processes have been observed in previous PROES experiments at this discharge [11, 15]. Heavy-particle collisional excitation is due to collisions of energetic (> 100 eV) hydrogen atoms with the background gas [11, 16]. The electron impact excitation processes can be explained on the basis of E-field measurements [17]. During the field-reversal phase —typical for hydrogen CCRF discharges— electrons are accelerated by the reversed electric field across the space charge sheath towards the powered electrode and induce strong impact excitation. When the sheath potential turns negative again, sheath expansion heating of electrons moving towards the plasma bulk occurs. Another excitation process is present during the phase of maximum hydrogen ion impact at the electrode surface [16]. Gamma electrons created at the surface are accelerated in the high sheath potential of several hundred Volts. Ionization by these electrons produces an avalanche of energetic directed secondary electrons towards the plasma bulk. In this work, the EEDFs during the field-reversal phase, the sheath expansion phase and the EEDF of secondary electrons are investigated.

The time dependencies of the excitation processes required for the presented analysis can be determined directly with eq. (1) from the population dynamics of the neon $2p_1$ state, since it is practically free of population by cascades [10]. Figure 1 displays the phase-resolved excitation close to the sheath boundary where all of the discussed electron impact excitation processes contribute. The time dependence of excitation during field reversal and sheath expansion can be approximated by triangular functions as indicated in the figure. The excitation by secondary electrons follows a squared sinusoidal function, since ion bombardment and acceleration in the sheath potential are both governed by sinusoidal functions.

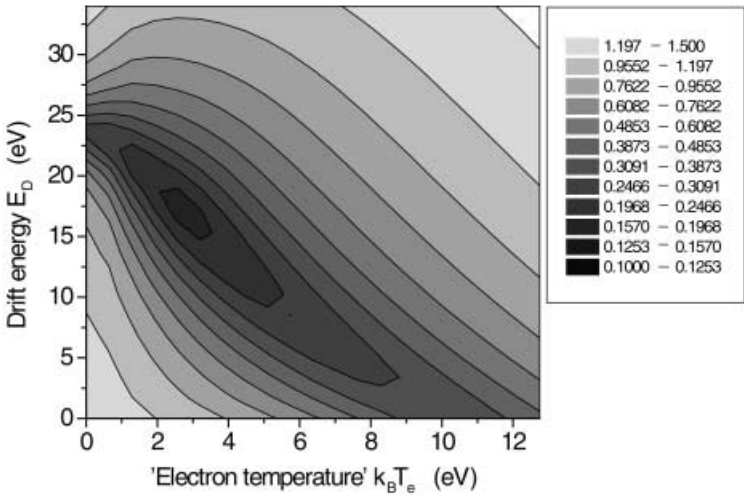

Fig. 2 – Deviation of measured and calculated excitation functions under variation of the free parameters at maximum excitation (approximately 1 mm in front of the powered electrode) during the field-reversal phase. The EEDF is obtained from the parameter set at minimum deviation.

An appropriate description of electrons in the discharge considered has to take into account a drift component in direction of the electric field in the sheath region. Distribution functions including this drift component were found to reproduce the measured excitation functions much better than the above-mentioned isotropic distribution functions. Tests with a 3-parameter anisotropic shifted Maxwellian distribution function (*i.e.* with two different "temperatures" in direction of the electric field and perpendicular) yielded the result that optimum agreement with measurements is always obtained when the two temperatures are almost identical. The further analysis is, therefore, based on a shifted Maxwellian distribution function $f_{\mathrm{D}}(E)$ with a drift energy E_{D} and a single temperature T_{e}:

$$f_{\mathrm{D}}(E) = \frac{1}{2\sqrt{\pi k_{\mathrm{B}} T_{\mathrm{e}} E_{\mathrm{D}}}} e^{-\frac{(\sqrt{E}-\sqrt{E_{\mathrm{D}}})^2}{k_{\mathrm{B}}T_{\mathrm{e}}}} \left(1 - e^{-\frac{4\sqrt{E}\sqrt{E_{\mathrm{D}}}}{k_{\mathrm{B}}T_{\mathrm{e}}}}\right). \tag{5}$$

Figure 2 shows an example of obtaining the parameter set which describes the EEDF at maximum excitation during the field-reversal phase. The deviation (defined as the standard deviation in percentage) of measured and calculated excitation functions under variation of the free parameters exhibits a clear minimum (15% standard deviation) indicating a strong drift component. Furthermore, the figure shows that the drift energy can be compensated partly by a higher electron temperature, but this results in larger deviations. It is very obvious when the drift energy is set equal to zero, which is equivalent to the assumption of a pure Maxwellian distribution function. In this case, the minimum deviation (on the abscissa) occurs at an electron temperature around 10 eV (> 30% standard deviation). The larger deviation by using a Maxwellian distribution function is a general problem of all isotropic distribution functions mentioned above. These functions decrease —in contrast to functions including a drift component— monotonically with energy in a plot like fig. 3. A decrease to lower energies cannot be described. The excitation of states with low threshold energies can, therefore, be overestimated by using these functions, which causes larger deviations. Figure 3 shows typical examples of EEDFs during the field-reversal phase, the sheath expansion phase and of secondary electrons. The strong influence of the drift component can be clearly seen. The ob-

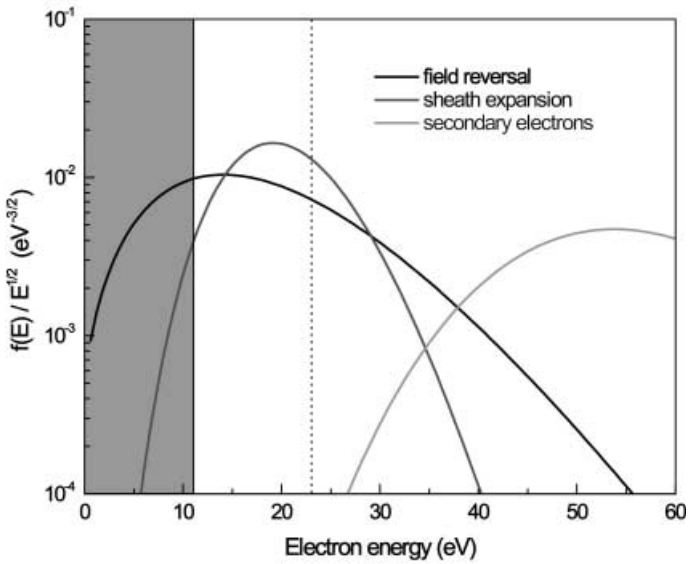

Fig. 3 – Typical examples of EEDFs during the field-reversal phase (at approximately 1 mm in front of the powered electrode), the sheath expansion phase and EEDF of secondary electrons (both at approximately 4 mm in front of the powered electrode). The lowest and highest excitation thresholds of the investigated states are indicated by vertical lines. The gray area is only accessible within the assumed functional behavior of the EEDF.

tained parameter sets describing the phase- and space-resolved EEDF are shown in fig. 4 for the various excitation processes at different phases of the RF cycle. From this representation both the drift energy and the electron temperature can be taken for each of the characteristic phases of the discharge cycle as a function of the distance from the powered electrode. In case of the secondary electrons the analysis tends to be unstable because of noisy data. However, only a weak dependence ($< 15\%$) of the drift energy is observable. The drift energy is, therefore, fixed

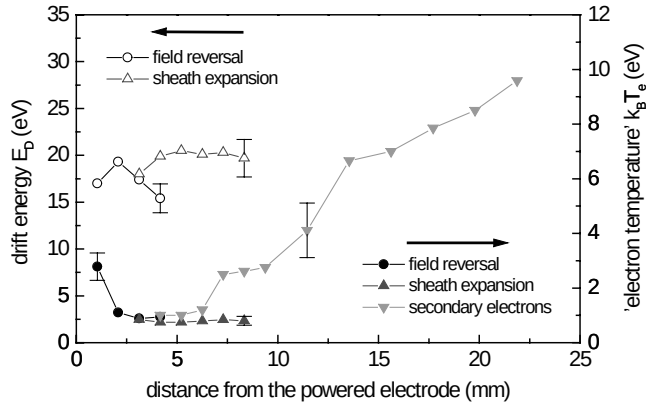

Fig. 4 – Parameter sets describing the phase- and space-resolved EEDF for the various excitation processes. For the secondary electrons the drift energy is fixed to 55 eV, see the text for details.

to the value obtained close to the sheath boundary ($E_D = 55\,eV$) to provide a stable analysis.

To summarize: We have presented a novel spectroscopic method for phase- and space-resolved measurements of the EEDF in RF discharges. The applicability was demonstrated at a hydrogen CCRF discharge at elevated pressure.

It is planned to apply this diagnostic beyond the present application to discharges in other gases, different pressure regimes and other types of RF discharges like inductively coupled plasmas and capacitively coupled dual-frequency plasmas. This will require to adapt the generalized distribution function approach in analogy to eq. (5) to the respective geometry.

* * *

The authors thank Prof. C. C. Lin (University of Wisconsin, Madison) for helpful discussions and C. Fischer and J. Leistikow for skilful technical assistance. Support by the DFG in the frame of SFB 191 is gratefully acknowledged.

REFERENCES

[1] Behringer K. and Fantz U., *J. Phys. D*, **27** (1994) 2128.
[2] Malyshev M. V. and Donnelly V. M., *Phys. Rev. E*, **60** (1999) 6016.
[3] Mahony C. M. O. and Graham W. G., *IEEE Trans. Plasma Sci.*, **27** (1999) 72.
[4] Hershkowitz N., *Plasma Diagnostics - Discharge Parameters and Chemistry*, Vol. **1** (Academic Press, San Diego) 1989.
[5] Godyak V. A., *Plasma - Surface Interaction and Processing of Materials, NATO ASI Ser. E*, Vol. **176** (1990) p. 95.
[6] Bowden M. D. *et al.*, *J. Appl. Phys.*, **73** (1993) 2732.
[7] Bogdanova I. P. and Yurgenson S. V., *Opt. Spektrosk.*, **61** (1986) 241.
[8] Chilton J. E. *et al.*, *Phys. Rev. A*, **57** (1998) 267.
[9] Chilton J. E., Stewart M. D. jr. and Lin C. C., *Phys. Rev. A*, **62** (2000) 32714.
[10] Chilton J. E., Stewart M. D. jr. and Lin C. C., *Phys. Rev. A*, **61** (2000) 52708.
[11] Gans T., Lin Chun C., Schulz-von der Gathen V. and Döbele H. F., *Phys. Rev. A*, **67** (2003) 012707.
[12] Katsch H. M., Quandt E. and Schneider Th., *Plasma Phys. Control. Fusion*, **38** (1996) 183.
[13] Gans T., Schulz-von der Gathen V. and Döbele H. F., *Plasma Sources Sci. Technol.*, **10** (2001) 17.
[14] NIST atomic spectra database, `http://physics.nist.gov/cgi-bin/AtData/main_asd`.
[15] Gans T., Lin Chun C., Schulz-von der Gathen V. and Döbele H. F., *J. Phys. D*, **34** (2001) L1.
[16] Gans T., Schulz-von der Gathen V., Czarnetzki U. and Döbele H. F., *Contrib. Plasma Phys.*, **42** (2002) 596.
[17] Czarnetzki U., Luggenhölscher D. and Döbele H. F., *Plasma Sources Sci. Technol.*, **8** (1999) 230.